PAMM

SPECIAL ISSUE 95th Annual Meeting of the International Association of Applied Mathematics and Mechanics (GAMM)

ORIGINAL PAPER OPEN ACCESS

Reduced Integration-Based Stabilization for Virtual Elements

Njomza Pacolli[1] | Jannick Kehls[1] | Mahmoud Sesa[1] | Stefanie Reese[1,2] | Hagen Holthusen[3]

[1]Institute of Applied Mechanics, RWTH Aachen University, Aachen, Germany | [2]University of Siegen, Siegen, Germany | [3]Institute of Applied Mechanics, University of Erlangen-Nuremberg, Erlangen, Germany

Correspondence: Njomza Pacolli (njomza.pacolli@ifam.rwth-aachen.de)

Received: 30 June 2025 | **Revised:** 27 October 2025 | **Accepted:** 10 November 2025

ABSTRACT

Stabilization techniques in combination with reduced integration are often employed in numerical methods to address problems of locking while reducing computational costs. In finite elements, concepts such as enhanced assumed strain (EAS) methods are usually employed in combination with stabilization techniques to tackle certain locking phenomena, such as volumetric or shear locking. This combination has been shown to improve the performance of low-order finite element formulations while addressing the downsides of reduced integration. In recent years, the virtual element method (VEM) has emerged as a numerical approach capable of handling arbitrary polygonal and polyhedral meshes, offering flexibility in mesh generation and refinement. This flexibility makes VEM particularly suitable for a wide range of applications involving distorted, non-convex, and irregular meshes. Similar to reduced integration, VEM formulations require stabilization to avoid rank deficiencies and ensure numerical consistency. Different stabilization techniques have been employed to overcome this issue. In this contribution, a stabilization technique based on reduced integration is proposed for VEM. The formulation is validated using two numerical examples.

1 | Introduction

The virtual element method (VEM) is an extension of the finite element method (FEM). It can handle arbitrary polygonal and polyhedral meshes, which do not necessarily need to be convex, offering flexibility in meshing, see first works in [1–3]. Advantages are shown especially in fields regarding crack propagation problems [4], contact problems [5], and mesh refinement procedures [6]. In comparison to FEM, VEM does not rely on an explicit computation of shape functions, nor is complex integration in the element needed [7]. Instead, it introduces a projection onto a polynomial subspace. However, this projection results in a rank-deficient stiffness matrix, and thus a stabilization term is needed. Several stabilization techniques have been developed for both linear and nonlinear problems, as discussed in, for example, [2, 7–11], or see the recently developed stabilization-free virtual elements, see [12–14]. In the context of FEM, stabilization techniques such as hourglass control [15, 16] are commonly employed to address issues that arise in combination with reduced integration, which is often applied to avoid locking phenomena. Locking is an underestimation of the displacements and an overestimation of the stresses, which occurs in the standard low-order finite element formulation using full integration. Typical examples of locking phenomena are volumetric locking for nearly incompressible materials or shear locking in bending-dominated problems, resulting in a stiff system. To tackle these issues, concepts such as the enhanced assumed strain method (EAS) are employed, where a two-field functional based on the Hu–Washizu variational principle is introduced [17, 18]. Reduced integration alone typically yields a rank-deficient matrix and leads to an overly soft structural response. To address this, some stabilization methods carry out a Taylor series expansion of the stress with respect to the center of the element, enabling analytical integration of the weak form, for example, [19–21]. Given that certain stabilization techniques apply to both FEM and VEM to avoid rank deficiencies, this

contribution proposes a stabilization method based on reduced integration combined with hourglass stabilization. Connections between VEM and hourglass control techniques have already been established in [22]. The main focus of this work is to conduct preliminary tests to investigate whether this approach yields plausible and reliable results considering simple geometries. To this end, numerical examples involving two-dimensional plane strain problems are presented to validate the proposed formulation.

2 | Virtual Element Formulation

2.1 | Consistency Term

The domain Ω of a body with its boundary Γ is divided into a mesh of polygonal elements Ω_v, each bounded by Γ_v. The elements do not necessarily have to be convex. The concept of the virtual element method lies in the approximation of the displacement $\boldsymbol{u}_h$ through a projection onto a polynomial subspace $\boldsymbol{u}_h \mapsto \Pi(\boldsymbol{u}_h) = \boldsymbol{u}_\pi$, since the ansatz of the displacement $\boldsymbol{u}_h$ within the virtual element remains unknown [2]. This leads to a split of the displacement into the so-called projection part $\boldsymbol{u}_\pi$ and a remaining part $\boldsymbol{u}_h - \boldsymbol{u}_\pi$

$$\boldsymbol{u}_h = \boldsymbol{u}_\pi + (\boldsymbol{u}_h - \boldsymbol{u}_\pi). \tag{1}$$

The projection is defined based on the orthogonality condition of the gradients. Due to the choice of a linear polynomial ansatz for $\boldsymbol{u}_\pi$, which implies a constant gradient over the element, this condition leads to the following expression for $\nabla \boldsymbol{u}_\pi$ [3, 8]

$$\nabla \boldsymbol{u}_\pi = \frac{1}{\Omega_v} \int_{\Omega_v} \nabla \boldsymbol{u}_h \, \mathrm{d}\Omega = \frac{1}{\Omega_v} \int_{\Gamma_v} \boldsymbol{u}_h \otimes \boldsymbol{N} \, \mathrm{d}\Gamma, \tag{2}$$

where $\boldsymbol{N}$ denotes the outward normal vector along the boundary Γ_v of the domain Ω_v. The displacement field $\boldsymbol{u}_h$ can be computed by a linear ansatz along the edges of the virtual element. For a more detailed derivation, see [9]. The derivations needed for the computation of the residual vector $\boldsymbol{R}_0$ and the stiffness matrix $\boldsymbol{K}_0 = \dfrac{\partial \boldsymbol{R}_0}{\partial \boldsymbol{U}}$, are obtained by using the automatic differentiation tool *JAX* [23], where $\boldsymbol{U}$ denotes the nodal displacement vector of the virtual element Ω_v.

2.2 | Stability Term

Due to the fact that the consistency term alone leads to a rank-deficient stiffness matrix, a stabilization term is needed, which is computed based on the remaining part of the split of the displacement, see Equation (1). For the sake of simplicity, the remainder is introduced as $\boldsymbol{u}^r$. The choice of the stabilization technique is based on the framework of using reduced integration with hourglass stabilization, see for example, [19, 24]. Here, the idea of using a Taylor series expansion of the constitutive quantities at the element center is employed.

In general, the two-field variational formulation based on the enhanced assumed strain concept (EAS) [17, 18] is defined as follows:

$$g_u^c(\boldsymbol{u}, \boldsymbol{w}, \delta\boldsymbol{u}) := \int_{\mathcal{B}_0} \boldsymbol{S}(\boldsymbol{E}) : \delta \boldsymbol{E}_c \mathrm{d}V - \int_{\mathcal{B}_0} \boldsymbol{f}_0 \cdot \delta\boldsymbol{u} \mathrm{d}V - \int_{\partial_t \mathcal{B}_0} \boldsymbol{t}_0 \cdot \delta\boldsymbol{u} \mathrm{d}A = 0, \tag{3a}$$

$$g_w(\boldsymbol{u}, \boldsymbol{w}, \delta\boldsymbol{u}) := \int_{\mathcal{B}_0} \boldsymbol{S}(\boldsymbol{E}) : \delta \boldsymbol{E}_{\mathrm{enh}} \, \mathrm{d}V = 0, \tag{3b}$$

where the total Green–Lagrange strain tensor $\boldsymbol{E}$, which is computed based on the remainder in Equation (1), is defined based on the split of the compatible part $\boldsymbol{E}_c$ and the enhanced part $\boldsymbol{E}_{\mathrm{enh}}$. For every virtual element domain Ω_v, a reference element is defined while the isoparametric concept is employed, where the (initial) geometry and displacement are discretized as follows:

$$\boldsymbol{x} \approx \boldsymbol{x}^h = \boldsymbol{N}(\boldsymbol{\xi}) \boldsymbol{X}, \qquad \boldsymbol{u}^r \approx (\boldsymbol{u}^r)^h = \boldsymbol{N}(\boldsymbol{\xi}) \boldsymbol{U}^r, \tag{4}$$

respectively. The element nodal positions and element nodal displacements based on the remainder are stored in vectors $\boldsymbol{X}$ and $\boldsymbol{U}^r$, respectively. The standard bilinear shape functions $\boldsymbol{N} = (N_1 \boldsymbol{I}_2, \dots, N_4 \boldsymbol{I}_2)$, depending on the natural coordinate vector $\boldsymbol{\xi} = (\xi, \eta)^T$ and the 2×2 identity tensor $\boldsymbol{I}_2$, are used. Based on this, the Jacobian matrix yields

$$\boldsymbol{J} = \frac{\partial \boldsymbol{x}}{\partial \boldsymbol{\xi}} \tag{5}$$

and the compatible Green–Lagrange strain tensor, depending on the remainder, is obtained as follows:

$$\boldsymbol{E}_c = \frac{1}{2} ((\boldsymbol{F}^r)^T \boldsymbol{F}^r - \boldsymbol{I}_2), \tag{6}$$

with $\boldsymbol{F}^r$ denoting the deformation gradient, while the compatible B-operator $\boldsymbol{B}_c$ is computed by using automatic differentiation (AD) and yields

$$\boldsymbol{B}_c = \frac{\partial \hat{\boldsymbol{E}}_c}{\partial \boldsymbol{U}} \tag{7}$$

with $\hat{\boldsymbol{E}}_c$ denoting the compatible Green–Lagrange strain in Nye's notation and $\boldsymbol{U}$ representing the nodal displacement vector. The enhanced assumed strain field in Nye's notation $\hat{\boldsymbol{E}}_{\mathrm{enh}}$ is computed based on the introduction of the incompatible B-operator $\bar{\boldsymbol{B}}_{\mathrm{enh}}$, which is defined in a way to overcome issues of shear locking depending on the natural coordinate system. Consequently, $\hat{\boldsymbol{E}}_{\mathrm{enh}}$ is obtained as follows:

$$\hat{\boldsymbol{E}}_{\mathrm{enh}} = \begin{bmatrix} 0 \\ 0 \\ E_{\mathrm{enh}\,\xi\eta} \end{bmatrix} = \boldsymbol{T}^0 \begin{bmatrix} 0 & 0 \\ 0 & 0 \\ \eta & \xi \end{bmatrix} \boldsymbol{W} = \boldsymbol{T}^0 \bar{\boldsymbol{B}}_{\mathrm{enh}} \boldsymbol{W} = \boldsymbol{B}_{\mathrm{enh}} \boldsymbol{W}. \tag{8}$$

The transformation matrix $\boldsymbol{T}^0$ evaluated at the element center contains the inverse Jacobian and transforms the enhanced B-operator to the Cartesian basis system, while $\boldsymbol{W}$ contains the two additional degrees-of-freedom, [17, 18]. Analogously, the same discretization holds for the variations $\delta\hat{\boldsymbol{E}}_c$ and $\delta\hat{\boldsymbol{E}}_{\mathrm{enh}}$. In the case of the concept of reduced integration, only a single Gauss point is used to overcome the issues of locking that arise with

using the standard low-order finite element formulation with full integration. To avoid the issues of a rank-deficient response, hourglass stabilization is used. The idea is to employ a Taylor series expansion of the constitutive quantities at the element center. This enables a polynomial representation of the stress, and thus analytical integration of the weak form is enabled. Consequently, the second Piola–Kirchhoff stress in Nye's notation $\hat{\boldsymbol{S}}$ is expressed as follows:

$$\begin{aligned}\hat{\boldsymbol{S}}(\hat{\boldsymbol{E}}) &\approx \hat{\boldsymbol{S}}\Big|_{\boldsymbol{\xi}=\boldsymbol{0}} + \boldsymbol{C}^{hg}\left(\sum_{i=1}^{2}\frac{\partial \hat{\boldsymbol{E}}}{\partial \xi_i}\Big|_{\boldsymbol{\xi}=\boldsymbol{0}}\xi_i + \frac{1}{2}\sum_{i=1}^{2}\sum_{\substack{j=1\\ j\neq i}}^{2}\left(\frac{\partial}{\partial \xi_j}\left(\frac{\partial \hat{\boldsymbol{E}}}{\partial \xi_i}\right)\right)\Big|_{\boldsymbol{\xi}=\boldsymbol{0}}\xi_i\,\xi_j\right)\\ &= \hat{\boldsymbol{S}}^0 + \boldsymbol{C}^{hg}\Big(\underbrace{\hat{\boldsymbol{E}}_c^{\xi}\,\xi + \hat{\boldsymbol{E}}_c^{\eta}\,\eta}_{=:\hat{\boldsymbol{E}}_c^{\mathrm{hg1}}} + \underbrace{\hat{\boldsymbol{E}}_c^{\xi\eta}\,\xi\eta}_{=:\hat{\boldsymbol{E}}_c^{\mathrm{hg2}}} + \underbrace{\hat{\boldsymbol{E}}_{\mathrm{enh}}^{\xi}\,\xi + \hat{\boldsymbol{E}}_{\mathrm{enh}}^{\eta}\,\eta}_{=:\hat{\boldsymbol{E}}_{\mathrm{enh}}}\Big)\\ &= \hat{\boldsymbol{S}}^0 + \underbrace{\boldsymbol{C}^{hg}(\hat{\boldsymbol{E}}_c^{\mathrm{hg1}} + \hat{\boldsymbol{E}}_c^{\mathrm{hg2}} + \hat{\boldsymbol{E}}_{\mathrm{enh}})}_{=:\hat{\boldsymbol{S}}^{\mathrm{hg}}}.\end{aligned} \tag{9}$$

Here, the superscript denotes the derivative with respect to the natural coordinates. Analogously, a polynomial form of both $\boldsymbol{B}_c$ and $\boldsymbol{B}_{\mathrm{enh}}$ is obtained. The material tangent is substituted with a linear elastic so-called hourglass tangent $\boldsymbol{C}^{hg}$ to circumvent linearization. Furthermore, $\boldsymbol{C}^{hg}$ is defined in a way such that $\hat{\boldsymbol{S}}^{\mathrm{hg}}$ has deviatoric characteristics to overcome volumetric locking. It is defined as follows:

$$\boldsymbol{C}^{hg} = \frac{\mu_{\mathrm{eff}}^{hg}}{3}\begin{bmatrix}4 & -2 & 0\\ -2 & 4 & 0\\ 0 & 0 & 3\end{bmatrix}, \quad \mu_{\mathrm{eff}}^{hg} = \frac{1}{2}\sqrt{\frac{\mathrm{tr}\left(\mathrm{dev}\left(\boldsymbol{S}^0\right)^2\right)}{\mathrm{tr}\left(\mathrm{dev}\left(\boldsymbol{E}_c^0\right)^2\right)}}, \tag{10}$$

with μ_{eff}^{hg} being the effective shear modulus. To circumvent linearization, μ_{eff}^{hg} is stored as a history variable and taken from the last converged step. With these derivations, the weak form can be derived analytically, where the residual vector $\boldsymbol{R}_{\mathrm{stab}}$ is obtained. For a more detailed explanation, see [25]. At the end, the stiffness matrix of the stabilization term is computed at the element level by AD as follows:

$$\boldsymbol{K}_{\mathrm{stab}} = \frac{\partial \boldsymbol{R}_{\mathrm{stab}}}{\partial \boldsymbol{U}}. \tag{11}$$

Finally, the residual vector and the stiffness matrix for the virtual element formulation yield

$$\boldsymbol{R} = \boldsymbol{R}_0 + \boldsymbol{R}_{\mathrm{stab}}, \quad \boldsymbol{K} = \boldsymbol{K}_0 + \boldsymbol{K}_{\mathrm{stab}}. \tag{12}$$

3 | Numerical Examples

The following two numerical examples serve to test the applied stabilization technique for the virtual element method. To this end, rectangular elements are used to investigate whether the proposed VEM formulation—referred to as VEM-STc+—exhibits stable and reliable behavior when compared to the traditional finite element method (FEM). For comparison, the standard low-order finite element formulation using full integration, denoted as Q1, and the low-order finite element formulation based on reduced integration with hourglass stabilization, denoted as Q1STc+, see [24], are used. In both examples, a large strain model is used, where a plane strain state is assumed, where a compressible neo-Hookean material model with the following Helmholtz free energy is chosen

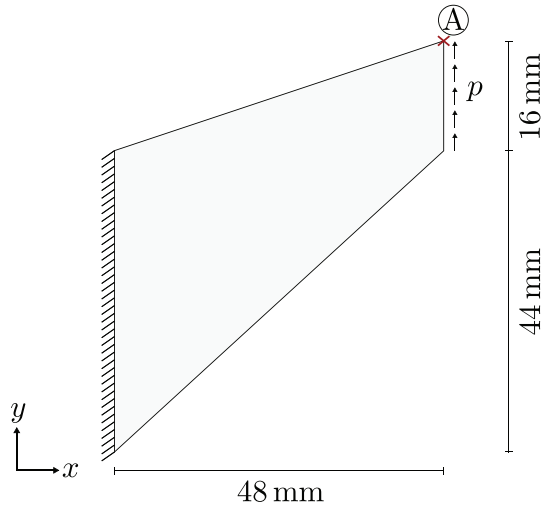

FIGURE 1 | Cook's membrane—Geometry and boundary value problem.

$$\psi = \frac{\mu}{2}\left(\mathrm{tr}\left(\boldsymbol{C}\right) - 3 - \ln\left(\det\left(\boldsymbol{C}\right)\right)\right) + \frac{\lambda}{4}\left(\det\left(\boldsymbol{C}\right) - 1 - \ln\left(\det\left(\boldsymbol{C}\right)\right)\right) \tag{13}$$

with $\boldsymbol{C}$ being the right Cauchy–Green tensor and λ and μ denoting the two Lamé constants. The results are measured in terms of the following relative error

$$\epsilon_u = \frac{|U_{\mathrm{conv}} - U_{\mathrm{obt}}|}{|U_{\mathrm{conv}}|}, \tag{14}$$

where U_{conv} denotes the converged solution obtained from the standard biquadratic finite element formulation, Q2. The obtained solution at a chosen point with VEM-STc+, Q1STc+, and Q1 is denoted by U_{obt}.

3.1 | Cook's Membrane

The first numerical example considered is Cook's membrane. The geometry and boundary value problem are shown in Figure 1. The structure is clamped along the left edge, while a constant vertical load of $p = 4\,\frac{\mathrm{N}}{\mathrm{mm}}$ is applied to the right edge in a single load step. The material parameters are $\lambda = 100.0\,\frac{\mathrm{N}}{\mathrm{mm}^2}$ and $\mu = 40.0\,\frac{\mathrm{N}}{\mathrm{mm}^2}$. A convergence study is conducted for the vertical displacement component U_y at the node (48,60), indicated by the red cross at point (A) in the figure. The results are shown in Figure 2a, where the converged solution $U_{\mathrm{conv}} = 9.9521\,\mathrm{mm}$ with a mesh density of 4096 elements was used to compute the relative error ϵ_u in a logarithmic scale for Q1, Q1STc+, and VEM-STc+. It can be seen that both Q1STc+ and VEM-Stc+ exhibit similar behavior regarding the development of the relative error as the number of elements per direction increases, with mesh densities defined by 2^N, where $N = 1, 2, 3, 4, 5, 6$. For both cases, the range of the relative error in a logarithmic scale lies between $\epsilon_u = 10^{-2}$ and $\epsilon_u = 10^{-4}$ for different mesh densities. It is worth mentioning that, in comparison to VEM-STc+, Q1STc+ shows a jump in the

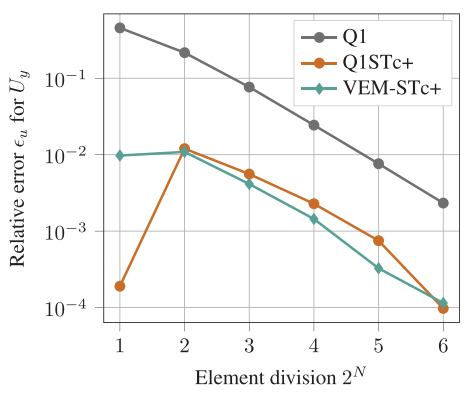

(a) Study of convergence at point A for U_y

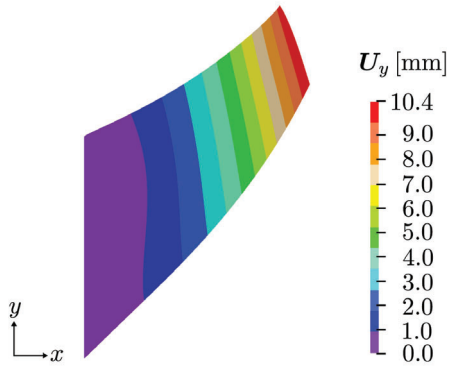

(b) Contour plot of U_y for VEM-STc+

FIGURE 2 | Cook's membrane—Study of convergence for the vertical displacement U_y at node (48,60), point (A) in Figure 1, along with the contour plot of the displacement field $\boldsymbol{U}_y$. Here, a converged solution $U_{\text{conv}} = 9.9521$ mm with a mesh density of 4096 elements is obtained using the standard biquadratic finite element formulation, Q2, to compute the relative error ϵ_u. The x-axis denotes the number of elements per direction, defined by 2^N with $N = 1, 2, 3, 4, 5, 6$. Results are presented for the standard low-order finite element formulation, Q1, the low-order finite element formulation based on reduced integration and hourglass stabilization, Q1STc+, and the proposed stabilization technique for the virtual element method, VEM-STc+.

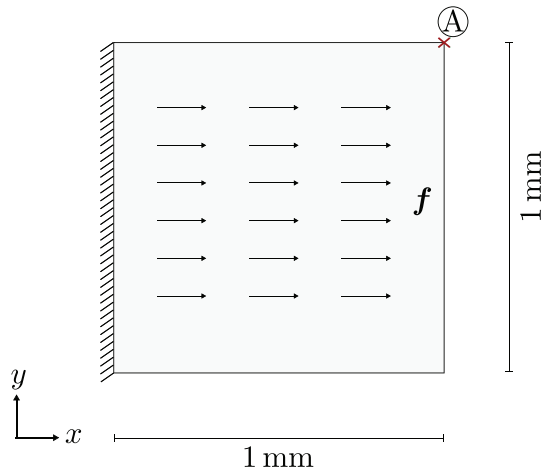

FIGURE 3 | Square block subjected to horizontal uniform body force—Geometry and boundary value problem.

error development between $N = 1$ and $N = 2$, where it initially starts small, then increases sharply, and then decreases in a stable fashion. The standard Q1 formulation shows a slower reduction in relative error with increasing mesh refinement. Figure 2b shows a contour plot of the vertical displacement field $\boldsymbol{U}_y$ for VEM-STc+.

3.2 | Square Block Subjected to Horizontal Uniform Body Force

The second example, taken from [8], considers a square block subjected to a horizontal uniform body force $\boldsymbol{f} = (10.5 \cdot 10^{10}, 0)^T \frac{\text{N}}{\text{mm}^3}$ while the structure is clamped at the left, see Figure 3a. The material parameters are $\lambda = 5.1086 \cdot 10^{10} \frac{\text{N}}{\text{mm}^2}$ and $\mu = 2.6316 \cdot 10^{10} \frac{\text{N}}{\text{mm}^2}$. To maintain consistency with the previous example, a convergence study is conducted for both the horizontal and vertical displacement components U_x and U_y at node (1,1) at point (A), see Figure 3a, with mesh densities defined by 2^N, where $N = 3, 4, 5, 6$. The results of Q1, Q1STc+, and VEM-STc+ are shown in Figure 4, where the converged solution of Q2 with $\boldsymbol{U}_{\text{conv}} = (U_x, U_y) = (1.121, -0.03488)$ (mm) and a mesh density of 16 900 elements was used to compute the relative error ϵ_u on a logarithmic scale. It can be seen that Q1STc+ and VEM-STc+ exhibit nearly identical behavior in Figure 4b, while Figure 4c shows differences in the error development, especially when considering a coarse mesh. However, as the mesh is refined, the relative error decreases, and VEM-STc+ progressively converges toward the results of Q1STc+. Here, for both figures, the relative error ϵ_u lies in the range between $\epsilon_u = 10^{-2}$ and $\epsilon_u = 10^{-4}$. As was the case in the first example, the standard Q1 formulation shows a slower reduction in relative error with increasing mesh refinement. Contour plots of the displacement fields $\boldsymbol{U}_x$ and $\boldsymbol{U}_y$ are shown for VEM-STc+ in Figure 5.

4 | Conclusion and Outlook

This contribution introduces a stabilization technique for the virtual element method (VEM) based on reduced integration combined with hourglass stabilization, referred to as VEM-STc+. To this end, hourglass stabilization of the remainder is applied, where a Taylor series expansion for the stress is carried out at the center of the element. The main objective was to conduct preliminary tests to investigate whether this approach yields plausible and reliable results, considering simple geometries. To this end, two numerical examples were presented: Cook's membrane and a square block subjected to a horizontal uniform body force. The results showed a similar convergence behavior for VEM-STc+ in comparison to Q1STc+. It is worth mentioning that VEM-STc+ would yield the same results as Q1STc+ if the stabilization term is not based on the remainder but rather replaced by solely the hourglass term in Q1STc+, $\boldsymbol{S}^{\text{hg}}$. With this, the consistency term in VEM is comparable to the constant term in the expansion in Q1STc+. In general, additional studies are required to assess mesh flexibility, as only convex rectangular elements were investigated in this work. Furthermore, a more detailed investigation of the formulation in terms of different, more complex numerical examples needs to

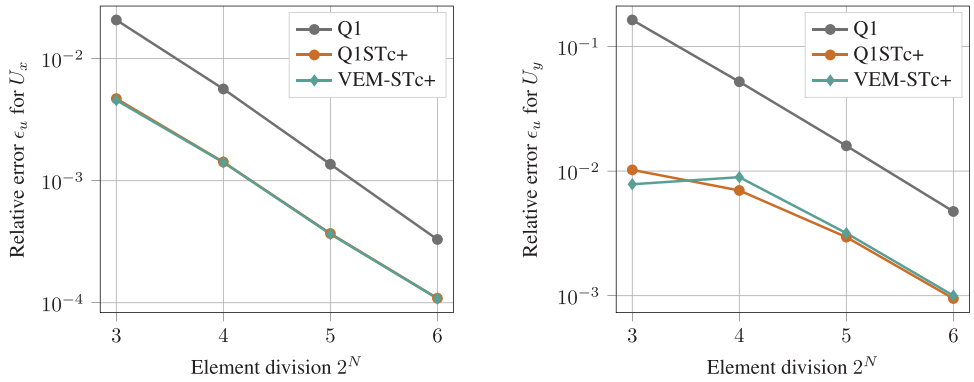

(a) Study of convergence at point A for U_x

(b) Study of convergence at point A for U_y

FIGURE 4 | Square block subjected to horizontal uniform body force—Study of convergence for the horizontal and vertical displacement U_x, U_y at node (1,1), point (A) in Figure 3a. Here, a converged solution $\boldsymbol{U}_{\text{conv}} = (U_x, U_y) = (1.121, -0.03488)\,(\text{mm})$ with a mesh density of 16 900 elements is obtained using the standard biquadratic finite element formulation, Q2, to compute the relative error ϵ_u. The x-axis denotes the number of elements per direction, defined by 2^N with $N = 3, 4, 5, 6$. Results are presented for the standard low-order finite element formulation, Q1, the low-order finite element formulation based on reduced integration and hourglass stabilization, Q1STc+, and the proposed stabilization technique for the virtual element method, VEM-STc+.

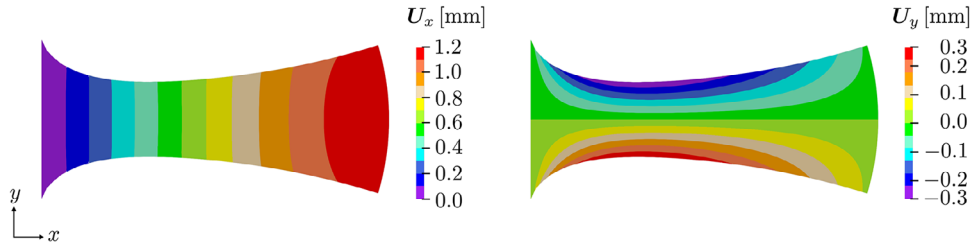

FIGURE 5 | Square block subjected to horizontal uniform body force—Countour plot of the displacement fields $\boldsymbol{U}_x$ and $\boldsymbol{U}_y$ for VEM-Stc+, see Figure 3a.

be conducted. Moreover, further analysis involving more complex numerical examples is essential to evaluate the robustness and applicability of the proposed formulation fully. Overall, the initial findings are encouraging and lay the groundwork for future research.

Acknowledgments

Hagen Holthusen and Stefanie Reese gratefully acknowledge financial support of the project 495926269 within the research unit FOR 5492 by the Deutsche Forschungsgemeinschaft. Stefanie Reese gratefully acknowledges the financial support of the research work B05 within SFB/TRR 339 with the project number: 453596084. Hagen Holthusen gratefully acknowledges the financial support of the research work by the Deutsche Forschungsgemeinschaft (DFG, German Research Foundation) within the transregional Collaborative Research Center SFB/TRR 280, project-ID 417002380.

Open access funding enabled and organized by Projekt DEAL.

References

1. L. Beirão da Veiga, F. Brezzi, A. Cangiani, G. Manzini, L. D. Marini, and A. Russo, "Basic Principles of Virtual Element Methods," *Mathematical Models and Methods in Applied Sciences* 23, no. 01 (2013): 199–214.

2. L. B. Da Veiga, F. Brezzi, and L. D. Marini, "Virtual Elements for Linear Elasticity Problems," *SIAM Journal on Numerical Analysis* 51, no. 2 (2013): 794–812.

3. L. Beirão da Veiga, F. Brezzi, L. D. Marini, and A. Russo, "The Hitchhiker's Guide to the Virtual Element Method," *Mathematical Models and Methods in Applied Sciences* 24, no. 08 (2014): 1541–1573.

4. A. Hussein, F. Aldakheel, B. Hudobivnik, P. Wriggers, P.-A. Guidault, and O. Allix, "A Computational Framework for Brittle Crack-Propagation Based on Efficient Virtual Element Method," *Finite Elements in Analysis and Design* 159 (July 2019): 15–32.

5. P. Wriggers, W. T. Rust, and B. D. Reddy, "A Virtual Element Method for Contact," *Computational Mechanics* 58, no. 6 (December 2016): 1039–1050.

6. D. vanHuyssteen, F. L. Rivarola, G. Etse, and P. Steinmann, "On Mesh Refinement Procedures for the Virtual Element Method for Two-Dimensional Elastic Problems," *Computer Methods in Applied Mechanics and Engineering* 393 (April 2022): 114849.

7. E. Artioli, L. Beirão da Veiga, C. Lovadina, and E. Sacco, "Arbitrary Order 2D Virtual Elements for Polygonal Meshes: Part I, Elastic Problem," *Computational Mechanics* 60, no. 3 (September 2017): 355–377.

8. L. Beirão da Veiga, C. Lovadina, and D. Mora, "A Virtual Element Method for Elastic and Inelastic Problems on Polytope Meshes," *Computer Methods in Applied Mechanics and Engineering* 295 (October 2015): 327–346.

9. P. Wriggers, B. D. Reddy, W. Rust, and B. Hudobivnik, "Efficient Virtual Element Formulations for Compressible and Incompressible Finite Deformations," *Computational Mechanics* 60, no. 2 (August 2017): 253–268.

10. H. Chi, L. B. daVeiga, and G. H. Paulino, "Some Basic Formulations of the Virtual Element Method (VEM) for Finite Deformations," *Computer Methods in Applied Mechanics and Engineering* 318 (May 2017): 148–192.

11. A. Lamperti, M. Cremonesi, U. Perego, A. Russo, and C. Lovadina, "A Hu–Washizu Variational Approach to Self-Stabilized Virtual Elements: 2D Linear Elastostatics," *Computational Mechanics* 71, no. 5 (May 2023): 935–955.

12. A. M. D'Altri, S. deMiranda, L. Patruno, and E. Sacco, "An Enhanced VEM Formulation for Plane Elasticity," *Computer Methods in Applied Mechanics and Engineering* 376 (April 2021): 113663.

13. A. Chen and N. Sukumar, "Stabilization-Free Virtual Element Method for Plane Elasticity," *Computers & Mathematics With Applications* 138 (May 2023): 88–105.

14. B.-B. Xu, Y.-F. Wang, and P. Wriggers, "Stabilization-Free Virtual Element Method for 2D Elastoplastic Problems," *International Journal for Numerical Methods in Engineering* 125, no. 15 (2024): e7490, _eprint: https://onlinelibrary.wiley.com/doi/pdf/10.1002/nme.7490.

15. T. Belytschko, J. S.-J. Ong, W. K. Liu, and J. M. Kennedy, "Hourglass Control in Linear and Nonlinear Problems," *Computer Methods in Applied Mechanics and Engineering* 43, no. 3 (1984): 251–276.

16. J. Bonet and P. Bhargava, "A Uniform Deformation Gradient Hexahedron Element With Artificial Hourglass Control," *International Journal for Numerical Methods in Engineering* 38, no. 16 (1995): 2809–2828.

17. J. C. Simo and F. Armero, "Geometrically Non-Linear Enhanced Strain Mixed Methods and the Method of Incompatible Modes," *International Journal for Numerical Methods in Engineering* 33, no. 7 (1992): 1413–1449.

18. J. Simo, F. Armero, and R. Taylor, "Improved Versions of Assumed Enhanced Strain Tri-Linear Elements for 3D Finite Deformation Problems," *Computer Methods in Applied Mechanics and Engineering* 110, no. 3 (1993): 359–386.

19. O. Barfusz, T. Brepols, T. van derVelden, J. Frischkorn, and S. Reese, "A Single Gauss Point Continuum Finite Element Formulation for Gradient-Extended Damage at Large Deformations," *Computer Methods in Applied Mechanics and Engineering* 373 (January 2021): 113440.

20. S. Reese, "On a Consistent Hourglass Stabilization Technique to Treat Large Inelastic Deformations and Thermo-Mechanical Coupling in Plane Strain Problems," *International journal for numerical methods in engineering* 57, no. 8 (2003): 1095–1127.

21. M. Schwarze and S. Reese, "A Reduced Integration Solid-Shell Finite Element Based on the EAS and the ANS Concept—Large Deformation Problems," *International Journal for Numerical Methods in Engineering* 85, no. 3 (2011): 289–329.

22. A. Cangiani, G. Manzini, A. Russo, and N. Sukumar, "Hourglass Stabilization and the Virtual Element Method," *International Journal for Numerical Methods in Engineering* 102, no. 3-4 (2015): 404–436, _eprint: https://onlinelibrary.wiley.com/doi/pdf/10.1002/nme.4854.

23. J. Bradbury, R. Frostig, P. Hawkins, et al., "JAX: Composable Transformations of Python+NumPy Programs," (2018).

24. N. Pacolli, A. Awad, J. Kehls, B. Sauren, S. Klinkel, S. Reese, and H. Holthusen, "An Enhanced Single Gaussian Point Continuum Finite Element Formulation Using Automatic Differentiation," *Finite Elements in Analysis and Design* 246 (April 2025): 104329.

25. M. Schwarze and S. Reese, "A Reduced Integration Solid-Shell Finite Element Based on the EAS and the ANS Concept—Geometrically Linear Problems," *International Journal for Numerical Methods in Engineering* 80, no. 10 (2009): 1322–1355, _eprint: https://onlinelibrary.wiley.com/doi/pdf/10.1002/nme.2653.